Paramagnetic Ionic Liquid-Coated $SiO_2@Fe_3O_4$ Nanoparticles - the Next Generation of Magnetically Recoverable Nanocatalysts Applied in the Glycolysis of PET

Israel Cano,*[§,ǂ] Carmen Martin,[†,ϕ] Jesum Alves Fernandes,[§] Rhys W. Lodge,[§] Jairton Dupont,[¥] Francisco A. Casado-Carmona,[‡] Rafael Lucena,[‡] Soledad Cardenas,[‡] Victor Sans[†,ψ] and Imanol de Pedro*[ϕ]

[§] School of Chemistry, University of Nottingham, NG7 2RD, Nottingham, UK.

[ǂ] Departamento de Física Aplicada, Facultad de Ciencias, Universidad de Cantabria, 39005 Santander, Spain

[†] GSK Carbon Neutral Laboratories for Sustainable Chemistry, Jubilee Campus, University of Nottingham, Nottingham, NG7 2GA, UK

[ϕ] CITIMAC, Facultad de Ciencias, Universidad de Cantabria, 39005 Santander, Spain

[¥] Laboratory of Molecular Catalysis, Institute of Chemistry, UFRGS, Av. Bento Gonçalves, 9500, Porto Alegre 91501-970, RS, Brazil.

[‡] Departamento de Química Analítica, Instituto de Química Fina y Nanoquímica. Edificio Marie Curie (anexo). Campus de Rabanales, Universidad de Córdoba, 14071 Córdoba, Spain

[ψ] Institute of Advanced Materials (INAM), Universidad Jaume I, 12006, Castellón, Spain

ABSTRACT: The functionalization of silica-coated, magnetic Fe_3O_4 nanoparticles, with an iron-containing ionic liquid, allows for the synthesis of a $Fe_3O_4@SiO_2@(mim)[FeCl_4]$ system that can be employed as a magnetically recoverable nanocatalyst. Herein, we present the use of $Fe_3O_4@SiO_2@(mim)[FeCl_4]$ for the glycolysis of PET into BHET under conventional heating. The catalyst achieved nearly 100% yield and selectivity over twelve consecutive reaction cycles at 180 °C and was efficiently recovered without tedious work-up or purification processes. Additional analyses revealed that the amount of catalyst lost after each cycle was negligible and no trace of Fe was found in the purified BHET product.

Keywords: Bifunctional catalyst • Bis(2-hydroxyethyl)terephthalate • Glycolysis • Imidazolium-based iron-containing ionic liquid • Poly(ethylene terephthalate) • magnetic nanoparticles

1. Introduction

Nowadays, polyethylene terephthalate (PET) is the fourth most manufactured plastic polymer, after polyethylene (PE), polypropylene (PP), and polystyrene (PS). The global PET production in 2014 amounted to some 42 million metric tons and it is predicted to increase to approximately 74 million

metric tons by 2020.[1] However, its manufacture and use presents many problems, including the requirement of non-renewable fossil fuel precursors, the astonishing amount of waste generated, and the CO_2 emissions related to both the production and disposal of PET products.[2] Therefore, the recycling of postconsumer PET is essential to save energy and protect our environment.[3]

Chemical recycling of PET waste involves the partial or total depolymerisation of this polymer into its monomers and oligomers, which can then be re-polymerised to yield recycled PET.[4] Common depolymerization routes employed for chemical recycling of PET are methanolysis, hydrolysis, glycolysis, aminolysis, ammonolysis and hydrogenation, among others.[5] In this context, glycolysis is a very convenient method due to its simplicity and low cost, but the non-catalysed process is very slow.[6] This transformation has been described by the use of a wide range of catalysts, such as metal acetates, titanium phosphate, solid superacids, carbonates, sulfates, deep eutectic solvents, nanoparticles, and microbial agents.[7,8,9,10,11] In particular, ionic liquids (ILs) have been increasingly explored as catalysts for PET glycolysis since the first report in 2009.[12] In a subsequent publication, Zhang et al. described the use of halometallate-based ILs for the depolymerization of PET in ethylene glycol (EG).[13] These acidic ILs operate as bifunctional catalysts acting simultaneously as a Lewis acid and nucleophile, showing higher activities and selectivities than those observed by the use of simple metal salts or solely organic ILs. Despite their advantages, in terms of selectivity and yield, only a few examples have been described where catalyst recovery is achieved employing expensive techniques, such as vacuum distillation.[14,15,16,17] If the catalyst recycling problem was solved, for example by immobilization using inorganic supports, halometallate-based ILs could be applicable in industrial processes. In this context, surface functionalization of magnetic nanoparticles (NPs) is an important and emerging area in the catalysis field.[18,19] Specifically, silica-coated magnetite nano-supports have attracted much attention due to their unique properties, such as chemical stability, non-toxicity, economic viability and simple preparation methods.[18] More importantly, retrieval of the NPs *via* magnetic separation provides an elegant alternative to cumbersome filtration, vacuum distillation, or centrifugation techniques in terms of time, energy and efficiency of catalyst retention.[20,21]

Inspired by these works, we report a new, highly active, bifunctional catalytic system, Fe_3O_4@SiO_2@(mim)[$FeCl_4$] (mim: methylimidazolium), that provides nearly 100% selectivity and yield in the glycolysis of PET in EG at T<180 °C. This thermally-stable, high-surface area nanocatalyst combines high activity with a facile magnetic recovery method and can be reused for up to 15 cycles. To the best of our knowledge, this is the first case which describes the surface modification of nano-magnetite materials with paramagnetic ILs (MILs), opening the door to the design of new nanomaterials with a wide range of possible functional groups in the shell. The depolymerization of PET catalyzed by magnetic NPs has been described for metal oxide spinel,[22] Mn_3O_4[23] and γ-Fe_2O_3.[24] However, the obtained BHET has often low purity and the required temperatures are higher (260-300 °C) than those used for this novel nanocatalyst.

2. Experimental

2.1. General Procedures

All reagents were purchased from Sigma Aldrich and purified when required by literature procedures.[25] PET pellets were supplied by Goodfellow Inc. (diameter 3–5 mm). Chemical shifts of ^{1}H and ^{13}C NMR are reported in ppm. Signals are quoted as s (singlet), t (triplet). Elemental analysis (EA) of Fe_3O_4@SiO_2@(mim)[$FeCl_4$] (**2**) was performed by the Elemental Analysis Service of the University of Nottingham (Nottingham, UK).

2.2. Instrumentation

2.2.1. Thermogravimetric analysis (TGA)

TGA measurements were carried out on a TA instruments Discovery at a heating rate of 10 °C/min in a temperature range from 25 °C to 800 °C under synthetic air in a platinum crucible.

2.2.2. Differential Scanning Calorimetry (DSC)

DSC measurements were carried out on a TA instruments Discovery from -90 to 150 °C at a rate of 10 °C/min under nitrogen atmosphere.

2.2.3. X-Ray Powder Diffraction (XRPD)

XRPD studies were performed in air atmosphere on a Bruker D8 Advance diffractometer, using Cu Kα radiation and a LynxEye detector. Diffraction patterns were collected with an angular 2θ range between 20° and 90° with a 0.05° step size and measurement time of 3 s per step, and a graphite monochromator. The instrumental resolution function (IRF) of the diffractometer was obtained from the LaB_6 standard.

2.2.4. Transmission electron microscopy (TEM) and high resolution transmission electron microscopy (HR-TEM)

TEM measurements were performed using a JEOL 2100F (field emission source, operated at 200 kV, information limit 0.19 nm). TEM samples were prepared by dissolving the samples in acetone, with brief sonication, before drop-casting the resulting mixture onto holey carbon, copper mesh TEM grids (Agar Scientific).

2.2.5. Energy-dispersive X-ray spectroscopy (EDX)

EDX was performed using an Oxford Instruments XMax 80 T silicon drift detector with INCA Energy 250 Microanalysis system.

2.2.6. X-ray photoelectron spectroscopy (XPS)

XPS measurements were performed using a Kratos AXIS Ultra DLD instrument. The chamber pressure during the measurements was 5×10^{-9} Torr. Wide energy range survey scans were collected at a pass energy of 80 eV in hybrid slot lens mode and a step size of 0.5 eV. High-resolution data on the C 1s, O 1s, N 1s, Cl 2p, Fe 2p, F 1s and P 2p photoelectron peaks were collected at a pass energy of 20 eV over energy ranges suitable for each peak (collection times of 5 min, step sizes of 0.1 eV). The charge neutraliser filament was used to prevent the sample charging over the irradiated area. The

X-ray source was a monochromated Al Kα emission, run at 10 mA and 12 kV (120 W). The energy range for each 'pass energy' (resolution) was calibrated using the Kratos Cu 2p3/2, Ag 3d5/2 and Au 4f7/2 three-point calibration method. The transmission function was calibrated using a clean gold sample method for all lens modes and the Kratos transmission generator software within Vision II. The data were processed with CASAXPS (Version 2.3.17). The high-resolution data were charge corrected to the reference C 1s alkyl chain signal at 284.8 eV.

2.2.7. Magnetic susceptibility measurements

Variable-temperature magnetic susceptibility measurements were performed using SQUID magnetometer heating from 2 to 300 K at several magnetic fields between 0.1 and 1 kOe after cooling in either the presence (field cooling, FC) or absence (zero field cooling, ZFC) of the applied field. Low-amplitude (h_{AC} = 1 Oe). Magnetization as a function of field (H) was measured using the same magnetometer in the $-50 \leq H/\text{kOe} \leq 50$ ranges at 300 and 2 K after cooling the sample at $H = 0$.

2.2.8. Fourier Transform Infrared Spectroscopy (FT-IR)

FT-IR measurement of BHET product was performed on a Bruker Alpha Series FT-IR spectrometer equipped with an attenuated total reflectance (ATR) module. The ATR FT-IR spectra were recorded by collecting 24 scans of a compound in the ATR module.

2.2.9. Nuclear Magnetic Resonance (NMR)

^{1}H and ^{13}C NMR spectra of BHET product was recorded on a Bruker DPX500 500 MHz nuclear magnetic resonance spectrometer.

2.2.10. Electrospray Ionization Mass Spectrometry (ESI-MS)

ESI-MS analyses of the BHET product were carried out on a Bruker ESI-TOF MicroTOF II.

2.2.11. Gas Chromatography Mass Spectrometry (GC-MS)

GC-MS analyses of the BHET product were performed on a Thermo Scientific ISQ-LT GC-MS equipped with a Single Quadrupole Mass Spectrometer and a ThermoScientific TG SQC column equivalent to DB5MS.

2.3. Synthesis of Paramagnetic Ionic Liquid-Coated SiO_2@Fe_3O_4 Nanoparticles

The synthesis of the Fe_3O_4 nanoparticles MNPs was performed in four stages following the literature procedure.[26] Next, the MNPs were coated with silica using tetraethylorthosilicate (TEOS) to obtain the silica-coated MNPs (Fe_3O_4@SiO_2),[27] followed by the functionalization of Fe_3O_4@SiO_2 with methylimidazolium-chloride.[26] The last step of the synthesis was the introduction of the paramagnetic ionic liquid onto the surface of the nanoparticles. For this purpose, Fe_3O_4@SiO_2@mim-Cl (2 g) was dispersed in an aqueous $FeCl_3$ solution (100 mL, 7% (w/v)) and the resulting mixture was stirred for 48 h to allow the substitution of the Cl^- by $FeCl_4^-$. The synthesized IL-MNPs, Fe_3O_4@SiO_2@(mim)[$FeCl_4$], were washed with Milli-Q water (50 mL), and dried at 80 °C for 8 h.

Elemental analysis (%): C, 3.54; H, 0.71; N, 0.71; Fe, 45.83.

TGA: 17.3% mass loss.

2.4. Catalytic experiments

2.4.1. General Procedure for Catalytic Degradation of PET

For the catalytic experiments, 15 mg of catalyst, 100 mg of PET and 1 mL of EG, were placed in a 10 mL round bottom flask equipped with a reflux condenser. The mixture was heated under reflux at 170 or 190 °C (160 and 180 ºC inside the reaction flask, respectively) for 24 h. After the specified time, the flask was cooled down to R.T. and 10 mL of distilled water were added to the reaction crude. The catalyst was separated from the aqueous phase with an external magnet and washed with distillated water two times. The different aqueous solutions were combined and the undepolymerized PET was separated from the resulting mixture and dried at 80 °C. The mixture was filtered and the liquid phase was evaporated at 72 mbar using a rotary evaporator at 40 °C to remove water. An aliquot of the residue (100 mg) was dissolved in DMSO-d_6 and analyzed by ^{1}H and ^{13}C NMR to determine the amount of BHET product using 1-phenyl-1,2-ethanediol (0.1 mmol) as an internal standard. The purity of the BHET product was confirmed using a wide range of techniques, such as XRPD, ^{1}H and ^{13}C NMR spectroscopy, ATR FT-IR, GC-MS, ESI-MS, elemental analysis (EA), DSC and TGA (*vide infra*, figures S22-S29 in Supporting Information). **^{1}H NMR** (500 MHz, 298 K, DMSO-d_6): δ 8.12 (s, 4H, CH_{Ar}), 4.96 (t, J = 5.7 Hz, 2H, –OCH$_2$CH$_2$O*H*), 4.32 (t, J = 4.9 Hz, 4H, –OCH_2CH$_2$OH), 3.72 (t, J = 5.2 Hz, 4H, –OCH$_2$CH_2OH). **^{13}C NMR** (126 MHz, DMSO-d_6): δ 165.2 (s, C_q, C=O), 133.7 (s, C_q, C_{Ar}), 129.5 (s, CH, C_{Ar}), 67.0 (s, –O*C*H$_2$CH$_2$OH), 59 (s, –OCH$_2$*C*H$_2$OH). **Characteristic IR bands** (cm^{-1}): 3444 (O-H), 2962 (C-H), 2945 (C-H), 2930 (C-H), 2879 (C-H), 1713 (C=O), 1503-1409 (C_{Ar}=C_{Ar}), 1275 (C-O), 1250 (O-H), 1070 (C-O), 909-860 (C_{Ar}=C_{Ar}). **HR-MS** (ESI+): m/z = 277.0677 (M + Na) (calculated: m/z = 277.0688) and m/z = 255.0860 (M + H$^+$) (calculated: m/z = 255.0869). **GC-MS** peak at 22.6, 254.93 (M + H$^+$), 210.99, 192.96, 148.97, 121.00, 104.03. **Anal. calcd. for $C_{12}H_{14}O_6$**: C 56.69, H 5.55; **found:** C 55.46, H 5.42.

The conversion of PET is calculated using the following equation:

$$\text{Conversion of PET} = \frac{W_0 - W_1}{W_0} \times 100 \qquad (1)$$

In which W_0 is the initial weight of PET and W_1 is the weight of undepolymerized PET. In addition, the yield and selectivity of BHET are defined by equations (2) and (3):

$$\text{Yield of BHET} = \frac{\text{moles of BHET}}{\text{initial moles of PET units}} \times 100 \qquad (2)$$

$$\text{Selectivity of BHET} = \frac{\text{moles of BHET}}{\text{moles of depolymerized PET units}} \times 100 \qquad (3)$$

2.4.2. General procedure for recycling experiments

15 mg of catalyst, 100 mg of PET and 1 mL of EG, were placed in a 10 mL round bottom flask equipped with a reflux condenser. The mixture was heated under reflux at 170 or 190 °C (160 and 180 ºC inside the reaction flask, respectively) for 24 h. After the specified time, the flask was cooled down to R.T. and 10 mL of distilled water were added to the reaction crude. The catalyst was separated from the aqueous phase with an external magnet and washed with distillated water two times. The different aqueous solutions were combined and the conversion of PET and the yield and selectivity of BHET was studied as previously described. The reaction flask containing the catalyst was dried using a rotary evaporator at 72 mbar and 40 °C to remove water. The catalyst was then used for the next cycle.

3. Results and discussion

3.1. Characterization of Fe_3O_4@SiO_2@(mim)[$FeCl_4$] Magnetic Nanoparticles

Fe_3O_4@SiO_2@mim-Cl (**1**) was obtained by a previously described protocol (for further details see section *2.3*).[27] Subsequently, 2 g of **1** were dispersed in 100 mL of 7% (w/v) $FeCl_3$ (aq) and stirred for 48 h, leading to the substitution of Cl^- by $FeCl_4^-$ in a simple step and the synthesis of Fe_3O_4@SiO_2@(mim)[$FeCl_4$] (**2**).

The nanostructured catalyst **2** has been extensively characterized by TGA, XRPD, TEM, EDX, HR-TEM, XPS, and magnetic measurements. TGA revealed that **2** is thermally stable up to 250 °C (Figure S1, Supporting Information), confirming the durability of the system at temperatures employed in the catalytic experiments. XRPD analysis (Figure S2, Supporting Information) showed the presence of magnetite (Fe_3O_4) and indicated that the mean NP diameter to be 9.2 nm. In addition, the XRPD spectrum of **2** presents a broad peak between 15 and 25° (2θ) that corresponds to the amorphous SiO_2@(mim)[$FeCl_4$] shells.[28] TEM analysis revealed the presence of well-dispersed and approximately-spherical nanoparticles with an average size *ca.* 11 ± 1 nm (Figures S6-S11, Supporting Information). Moreover, HR-TEM images (Figure 1) showed crystalline nanoparticles compatible with the characteristic face centered cubic (fcc) pattern for Fe_3O_4 crystals viewed along with the [311] axis with predominant lattice fringe distance of 0.253 nm (core) covered by an amorphous layer of SiO_2@(mim)[$FeCl_4$] of ranging between 0.5–2.0 nm in thickness. The observed thickness of the silica (Figure 1b) also depends on the angle that the particle is imaged at. For example, tilting of the TEM sample holder through 20° in the x-axis showed that the apparent thickness could decrease by approximately 20% (See figure S12, Supporting Information).

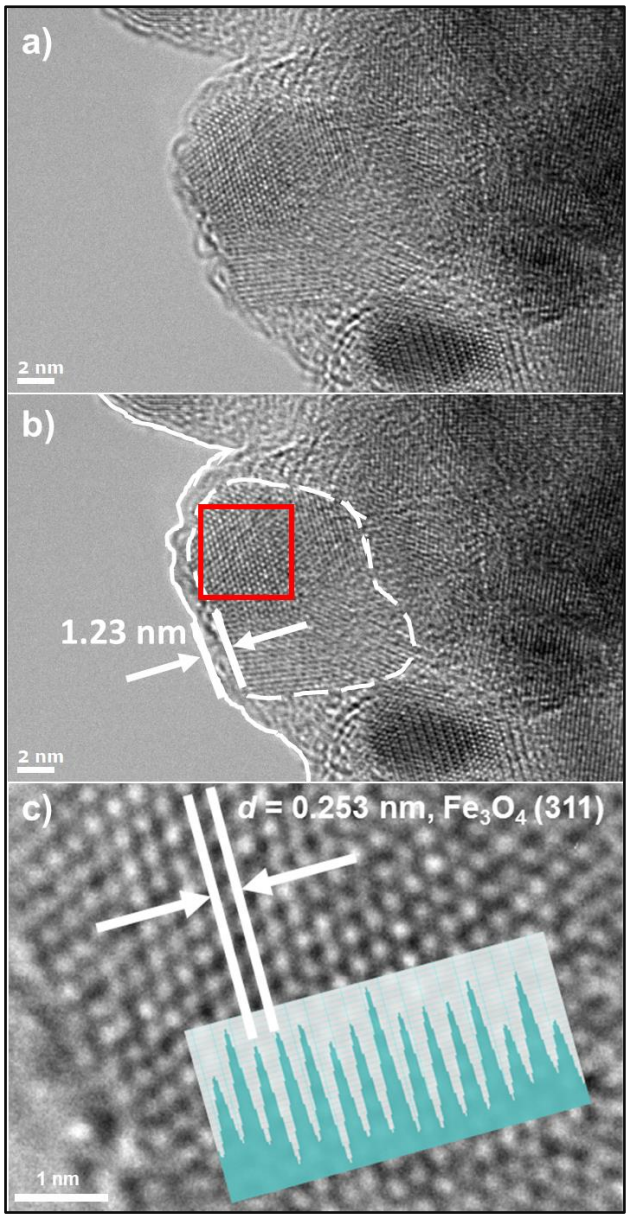

Figure 1. HR-TEM micrographs of the Fe_3O_4 NPs showing the discrete NPs on the silica support (a); the amorphous layer of SiO_2@(mim)[$FeCl_4$] (b); and the (311) interplanar spacing confirming Fe_3O_4 (c).

XPS measurements confirmed the presence of the imidazolium cation in the shell (Figure 2a). The Fe $2p_{3/2}$ signal (Figure 2c) was deconvoluted into two components associated to Fe^{2+} (709.4 eV) and Fe^{3+} (712.4 eV), which correspond to Fe_3O_4 oxidation states[29] and are in agreement with XRPD and HRTEM results. The signal associated with $FeCl_4$ overlaps with a very intense Fe_3O_4 NP core signal, but the Cl 2p signal suggested the presence of a thin $FeCl_4$ layer on the nanoparticle surface (Figure 2b). Indeed, EDX corroborated the presence of Fe, Cl, Si and O in the sample (Figure S14, Supporting Information). In addition, a STEM-EDX elemental map over a single Fe_3O_4@SiO_2@(mim)[$FeCl_4$] particle (Figures S15 and S16) showed the presence of Fe, Cl, Si and O in the shell, proving the

presence of the iron-containing ionic liquid in the surface of Fe_3O_4@SiO_2. Elemental analysis gave a halometallate-based IL content of *ca*. 20.6% in **2**, which is supported by TGA (*ca*. 17.3%, see figure S1, Supporting Information).

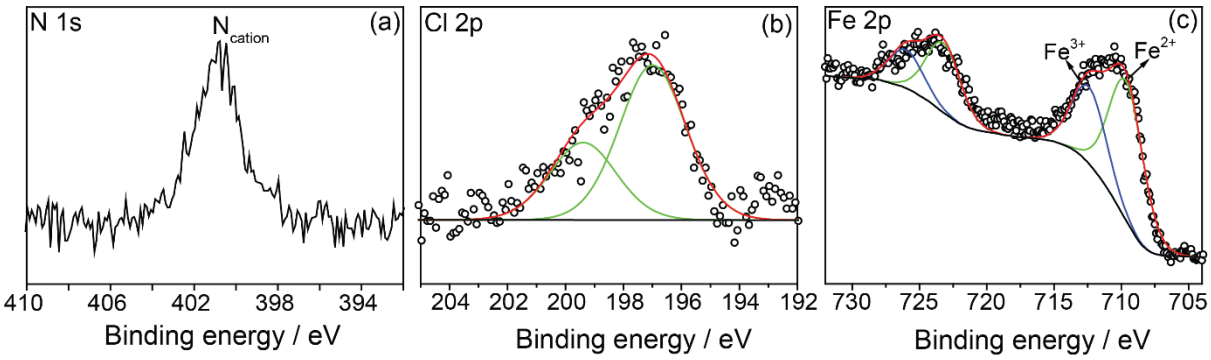

Figure 2. XPS analysis of N 1s, Cl 2p and Fe 2p, signals of Fe_3O_4@SiO_2@(mim)[$FeCl_4$] (**2**).

The magnetic susceptibility measurements as a function of temperature (Figure S17a, Supporting Information) showed typical features of single domain nanoparticles with a broad size distribution due to random dipolar interactions. The magnetic analysis (Section 6, Supporting Information) proved that a spin glass (SG)-like, rather than superparamagnetic freezing, seems to be occurring within the sample. Moreover, the response of magnetization to the applied magnetic field (Figure S17b, Supporting Information) is characteristic of an assembly of NPs. Finally, the fitting of the M(H) curves with the numerical inversion method[30] (Figure S18, Supporting Information) provided a value for the average size of 9.3 ± (1) nm, in good agreement with XRPD and TEM data.

3.2. Catalytic Glycolysis of PET by Fe_3O_4@SiO_2@(mim)[$FeCl_4$] Magnetic Nanoparticles

The catalytic activity of Fe_3O_4@SiO_2@(mim)[$FeCl_4$] MNPs (**2**) was evaluated for the glycolysis of PET in EG under conventional heating conditions (for further details see section *2.4.1*). We employed PET pellets purchased from Goodfellow Inc. (diameter 3–5 mm). The BHET product was obtained with high purity (Figures S20 and S21, Supporting Information) by crystallization in water at 4 °C (for further details see section *2.4.1*). This was confirmed using a wide range of techniques, such as TGA, DSC, FT-IR, XRPD, ESI-MS, ^{1}H and ^{13}C NMR, and GC-MS (Section 8 and figures S22-S29, Supporting Information). Moreover, no traces of Fe were found in the purified product by scanning electron microscope (SEM), which proves the suitability of the described procedure to obtain highly pure BHET that can be employed in subsequent applications.

The first set of experiments was carried out with a reaction temperature of 170 °C (160 °C inside the reaction flask). The conversion of PET and the yield of BHET product reached up to 63 and 59%, respectively (Figure 3). The comparison of these results with those observed for the analogous non-supported halometallate-based IL (dimim)[$FeCl_4$] at the same temperature (99% conversion and 78% yield for 0.085 mmol catalyst and 125 mg PET)[31] indicates that the activity of **2** is lower. However,

we have to bear in mind that the catalyst loading is a crucial factor in the glycolysis of PET[16] and the amount of catalytically active material is much lower in **2** (*ca*. 0.01 mmol of MIL in 15 mg of 2 employed for 100 mg PET), since the catalyst is present only in the shell of Fe_3O_4@SiO_2@(mim)[$FeCl_4$] NPs. Furthermore, we observed a significant decrease in the activity in the second cycle of catalyst recovery and reuse for (dimim)[$FeCl_4$] (from 99 to 5% yield) due to a gradual loss and/or decomposition of the catalyst as a consequence of the repeated washing cycles.[31] However, the nanocatalyst **2** was magnetically recyclable in 3 min (Figure 4, for further details see section *2.4.2*), which represents an easy retrieval method compared to the tedious and expensive procedures mentioned previously. Indeed, the recovered nanocatalyst was reused for up to fifteen cycles at 160 °C showing good recycling performance (Figure 3). In addition, a variable activity was observed for the different cycles. At this temperature, unreacted or partly reacted polymer was adsorbed on the nanoparticle surface, which hinders the complete separation of the catalyst from substrate and products during the recycling process, and thus leads to a fluctuation in the results. This has been demonstrated by performing a TGA of the nanoparticles after reaction at 160 ºC (Figure S40), which shows a 16.4% of adsorbed organic material.

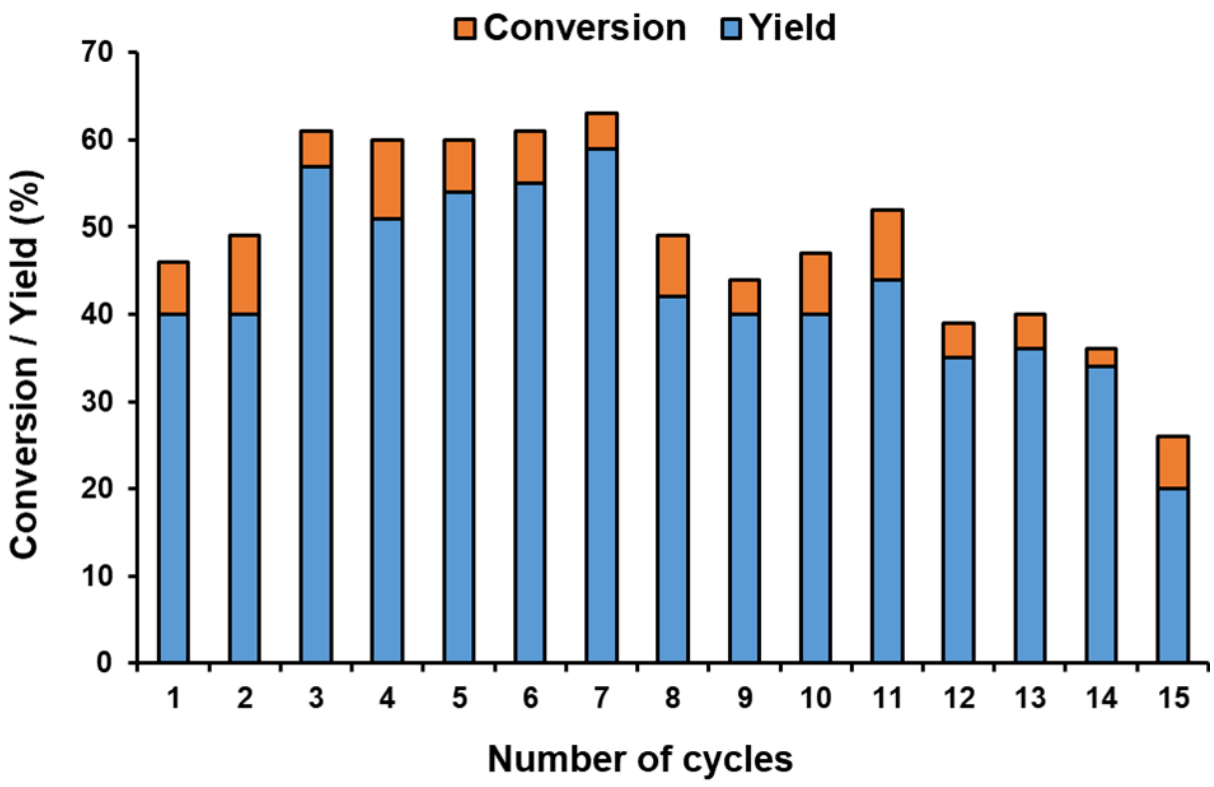

Figure 3. Reuse of Fe_3O_4@SiO_2@(mim)[$FeCl_4$] (**2**) in the glycolysis of PET. Reagent and conditions: catalyst (15 mg), PET (100 mg), EG (1 mL), 170 °C (160 °C inside the reaction flask), 24 h.

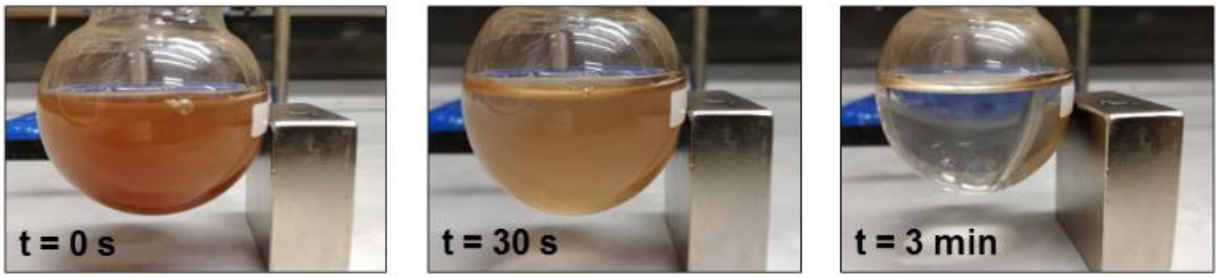

Figure 4. Magnetic separation of **2** employing an external magnet.

The catalytic activity of **2**, containing a Lewis acid and a nucleophile within the structure, was also compared with that observed for ILs supported on NPs. To this end, Fe_3O_4@SiO_2@(mim)[PF_6] NPs (**3**) of 11 ± (1) nm were synthesized and characterized by XRPD, TEM and XPS (Figures S3, S13 and S19, Supporting Information).[27] Although **3** exhibits similar recycling behavior as **2**, and can be reused up to 15 cycles (Figure S30, Supporting Information), the reaction showed lower activity (up to 40% conversion of PET and 36% yield of BHET), thus proving the importance of the halometallate complex in the catalytic process. The reaction mechanism in the glycolysis of PET catalysed by **2** is well aligned with that accepted for PET degradation mediated by imidazolium-based metal-containing ionic liquids, which is a Lewis acid catalytic process;[14,15,16] both the imidazolium cation and metal complex anion play a key synergic role through hydrogen-bonding interactions with EG and the ester groups of PET,[32] leading to enhanced activities and selectivities compared to those observed for purely organic imidazolium-based ILs.[13,31]

The reaction temperature is a critical factor in the glycolysis of PET catalyzed by ILs where higher temperatures favor the formation of BHET.[12] As **2** is stable up to 220 °C, another set of glycolysis reactions with the same experimental setting were carried out at 190 °C (180 °C inside the reaction flask). Interestingly, the activity of **2** improved significantly and, as can be seen in figure 5, quantitative conversions of PET and yields of BHET product were obtained. Conversely, the analogous non-supported iron-containing IL (dimim)[$FeCl_4$] only gave 80% conversion and 50% yield under the same reaction conditions. More importantly, catalyst **2** was reused up to twelve cycles without any significant loss in the catalytic activity and with only a slight decrease in the selectivity, showing an excellent recycling behavior.

Comparing with other systems based on a non-expensive and abundant metallic element such as iron, Pingale and coworkers described 63% yield of BHET at 197 ºC in the glycolysis of postconsumer PET bottle waste catalysed by $FeCl_3$ (EG, 7 h, 0.5% $FeCl_3$ w/w), but the catalytic system was not reused.[33] Similarly, Zhang *et al.* employed the iron-containing ionic liquid (bmim)[$FeCl_4$] (bmim = 1-butyl-3-methylimidazolium) for PET degradation.[13] This non-reusable catalyst gave quantitative conversion of PET and 59.2% selectivity towards BHET in 4 h at 178 ºC. In the field of magnetic nanoparticles, Kim and coworkers described superparamagnetic γ-Fe_2O_3 NPs of 10.5 nm in size as a recyclable catalyst for the glycolysis of PET.[24] This nanocatalyst was reused for up to 10 cycles,

leading to the formation of BHET product with >90% yield in 60 min at 300 ºC (0.05 catalyst/PET weight ratio) and >80% yield in 80 min at 255 ºC (0.10 catalyst/PET weight ratio). In addition, Al-Sabagh *et al.* reported quantitative yields at 190 ºC for eight cycles in PET glycolysis employing a binary catalyst consisting of Fe_3O_4 NPs and multi walled carbon nanotubes (MWCNTs).[11]

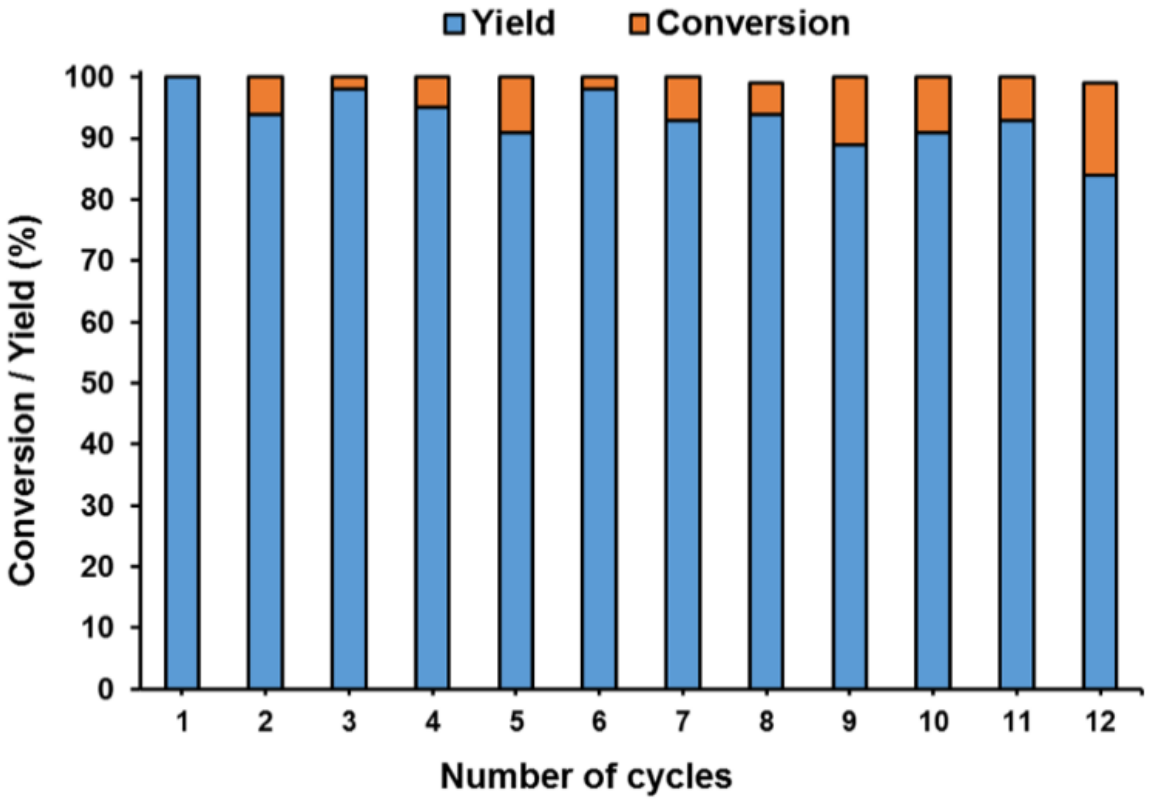

Figure 5. Recyclability of **2**. Reagent and conditions: catalyst (15 mg), PET (100 mg), EG (1 mL), 190 °C (180 °C inside the reaction flask), 24 h.

The magnetic separation method is very simple and highly efficient; further analyses by ICP revealed that the amount of catalyst lost after each cycle was only 1.7% of the total mass. The recovered catalyst was analyzed by TEM (Figure 6 and figures S33-S38, Supporting Information), showing the presence of nanoparticles with a SiO_2 coating and similar size to **2**. EDX confirmed the presence of Fe, Cl, Si and O belonging to the layer of SiO_2@(mim)[$FeCl_4$] in the shell of the nanoparticles (Figure S39, Supporting Information). Additionally, no appreciable differences were observed between the TGA of recovered catalyst with that of non-used Fe_3O_4@SiO_2@(mim)[$FeCl_4$], (Figure S41, Supporting Information). Likewise, the high resolution XPS spectra of Fe 2p for Fe_3O_4@SiO_2@(mim)[$FeCl_4$] before and after the recycling experiments are very similar. Indeed, the Fe 2p signal displayed the same binding energy and valence state ratios (Figures S42 and S43, Supporting Information).

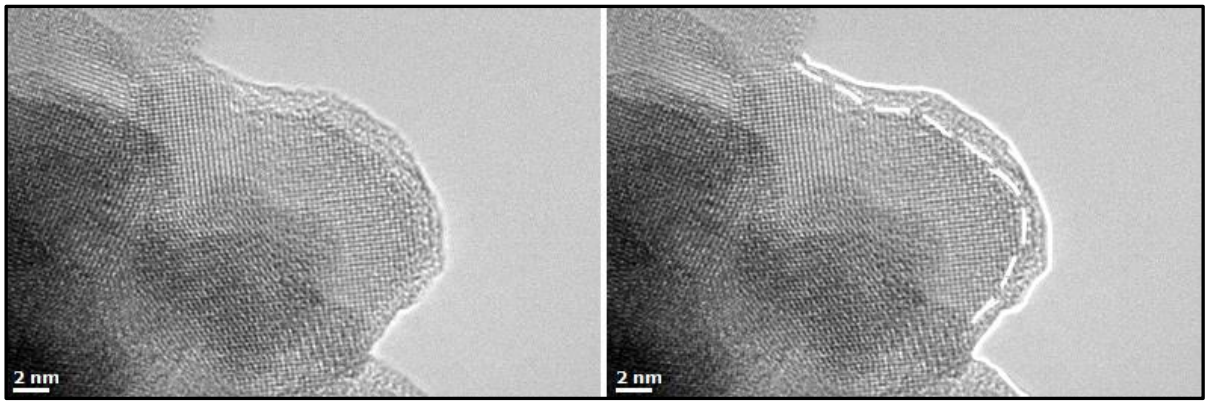

Figure 6. TEM image of Fe_3O_4@SiO_2@(mim)[$FeCl_4$] (**2**) recovered after catalytic reaction.

Finally, a set of control experiments under the same conditions was carried out to investigate the importance of nanocatalyst **2** in the catalytic process. First, no reaction was observed in the absence of catalyst. Next, Fe_3O_4@SiO_2@mim-Cl (**1**) and Fe_3O_4@SiO_2@(mim)[PF_6] (**3**) NPs showed good recycling performance but with lower activity (Figures S31 and S32, Supporting Information). Finally, bare Fe_3O_4 NPs of 12.1 ± (1.7) nm in size (Figure S4, Supporting Information) and Fe_3O_4@SiO_2 NPs of 29 ± (4) nm (12.0 nm diameter in the Fe_3O_4 core; figure S5, Supporting Information), gave considerably lower yields (98% PET conversion and 32% BHET yield for Fe_3O_4; 66% PET conversion and 62% BHET yield for Fe_3O_4@SiO_2). Thus, these results confirmed the crucial role of halometallate-based IL shell in the PET degradation process.

As shown in the present study, this new type of nanocatalyst displays very interesting features in terms of Lewis-acidity, activity, selectivity, stability, recovery, recyclability, and capacity for tuning with a wide range of halometallate-based IL shell.[34,35,36,37,38] Consequently, they could be very useful for other reactions catalyzed by halometallate-based ILs, such as glycosidation,[39] Michael addition, [40] desulfurization,[41] CO_2 fixation into cyclic carbonates,[42,43] Friedel Crafts acylation,[44] and benzylation of arenes into diarylmethanes.[45]

4. Conclusions

In summary, a halometallate-based IL was immobilized on the surface of Fe_3O_4@SiO_2 NPs *via* a simple and accessible procedure. The resulting Fe_3O_4@SiO_2@(mim)[$FeCl_4$] MNPs were fully characterized by the use of a wide variety of techniques. This bifunctional catalytic system showed very high activity for the glycolysis of PET, leading to quantitative yields of BHET monomer at 180 °C. Importantly, the system exhibits an excellent recycling behavior and can be easily recovered with an external magnetic field. Indeed, this nanocatalyst was reused for up to twelve cycles at 180 °C without any significant loss in the catalytic activity (84% yield of BHET in the twelfth run). Furthermore, the catalytic system remained active in the fifteenth cycle of recovery and reuse at 160 °C. Additional studies showed that the amount of catalyst lost after each cycle was minimal,

proving the efficacy of the magnetic separation procedure. The absence of even trace amounts of Fe in the purified product further illustrates the benefits of the described methodology to obtain highly pure BHET for potential reuse.

In conclusion, a new type of nanocatalyst with very exciting properties in terms of Lewis-acidity, stability, magnetism and capacity of tuning with a wide range of organic and inorganic compounds has been devised. In this first application the catalytic system was employed in the PET degradation process, but after this thorough study the road seems open for many catalytic reactions mediated by halometallate-based ILs.

Acknowledgments

Financial support from Universidad de Cantabria (Proyecto Puente convocatoria 2018 financed by SODERCAN_FEDER) and Spanish Ministry of Economy Industry and Competitiveness (Grant No. CTQ2017-83175R). Israel Cano acknowledges financial support from the European Community through a Marie Skłodowska-Curie Individual Fellowships (IF-EF; Programme/Call: H2020-MSCA-IF-2015; Proposal No: 704710–Sdchirnanocat). The authors would also like to acknowledge the Nanoscale and Microscale Research Centre at the University of Nottingham for access to their TEM facilities. Victor Sans acknowledges the Generalitat Valenciana (CIDEGENT/2018/036) for funding.

Appendix A. Supplementary data

TGA and Rietveld analysis, XPS and magnetic data and analysis, TEM images, characterization of BHET monomer and recycling experiments. Supplementary data associated with this article can be found, in the online version

Notes and References

[1] U.T. Bornscheuer, Feeding on plastic, Science 351 (2016) 1154-1155.
[2] C.M. Rochman, M.A. Browne, B.S. Halpern, B.T. Hentschel, E. Hoh, H.K. Karapanagioti, L.M. Rios-Mendoza, H. Takada, S. Teh, R.C. Thompson, Policy: classify plastic waste as hazardous, Nature, 494 (2013) 169-171.
[3] F. Welle, Twenty years of PET bottle to bottle recycling—an overview, Resour. Conserv. Recy. 55 (2011) 865-875.
[4] C. Gioia, M. Vannini, P. Marchese, A. Minesso, R. Cavalieri, M. Colonna, A. Celli, Sustainable polyesters for powder coating applications from recycled PET, isosorbide and succinic acid, Green Chem. 16 (2014) 1807-1815.
[5] N. George, T. Kurian, Recent developments in the chemical recycling of postconsumer poly(ethylene terephthalate) waste, Ind. Eng. Chem. Res. 53 (2014) 14185-14198.
[6] K. Troev, G. Grancharov, R. Tsevi, I. Gitsov, A novel catalyst for the glycolysis of poly(ethylene terephthalate), J. Appl. Polym. Sci. 90 (2003) 1148-1152.
[7] V.K. Sinha, M.R. Patel, J.V. Patel, PET waste management by chemical recycling: a review, J. Polym. Environ. 18 (2010) 8-25.
[8] S.K. Kale, A.G. Deshmukh, M.S. Dudhare, V.B. Patil, Microbial degradation of plastic: a review, J. Biochem. Tech. 6 (2015) 952-961.

[9] B. Liu, W. Fu, X. Lu, Q. Zhou, S. Zhang, Lewis acid−base synergistic catalysis for polyethylene terephthalate degradation by 1,3-dimethylurea/$Zn(OAc)_2$ deep eutectic solvent, ACS Sustainable Chem. Eng. 7 (2019) 3292-3300.
[10] F.R. Veregue, C.T.P. da Silva, M.P. Moisés, J.G. Meneguin, M.R. Guilherme, P.A. Arroyo, S.L. Favaro, E. Radovanovic, E.M. Girotto, A.W. Rinaldi, Ultrasmall cobalt nanoparticles as a catalyst for PET glycolysis: a green protocol for pure hydroxyethyl terephthalate precipitation without water, ACS Sustainable Chem. Eng. 6 (2018) 12017-12024.
[11] A.M. Al-Sabagh, F.Z. Yehia, D.R.K. Harding, Gh. Eshaq, A.E. ElMetwally, Fe_3O_4-boosted MWCNT as an efficient sustainable catalyst for PET glycolysis, Green Chem. 18 (2016) 3997-4003.
[12] H. Wang, Y. Liu, Z. Li, X. Zhang, S. Zhang, Y. Zhang, Glycolysis of poly(ethylene terephthalate) catalyzed by ionic liquids, Eur. Polym. J. 45 (2009) 1535-1544.
[13] H. Wang, R. Yan, Z. Li, X. Zhang, S. Zhang, Fe-containing magnetic ionic liquid as an effective catalyst for the glycolysis of poly(ethylene terephthalate), Catal. Commun. 11 (2010) 763-767.
[14] X. Zhou, X. Lu, Q. Wang, M. Zhu, Z. Li, Effective catalysis of poly(ethylene terephthalate) (PET) degradation by metallic acetate ionic liquids, Pure Appl. Chem. 84 (2012) 789-801.
[15] Q. Wang, X. Lu, X. Zhou, M. Zhu, H. He, X.P. Zhang, 1-Allyl-3-methylimidazolium halometallate ionic liquids as efficient catalysts for the glycolysis of poly(ethylene terephthalate), J. Appl. Polym. Sci. 129 (2013) 3574-3581.
[16] Q. Wang, Y. Geng, X. Lu, S. Zhang, First-row transition metal-containing ionic liquids as highly active catalysts for the glycolysis of poly(ethylene terephthalate)(PET), ACS Sustainable Chem. Eng. 3 (2015) 340-348.
[17] A.M. Al-Sabagh, F.Z. Yehia, Gh. Eshaq, A.E. ElMetwally, Ionic liquid-coordinated ferrous acetate complex immobilized on bentonite as a novel separable catalyst for PET glycolysis, Ind. Eng. Chem. Res. 54 (2015) 12474-12481.
[18] M.B. Gawande, P.S. Branco, R.S. Varma, Nano-magnetite (Fe_3O_4) as a support for recyclable catalysts in the development of sustainable methodologies, Chem. Soc. Rev. 42 (2013) 3371-3393.
[19] M. Zhu, G. Diao, Review on the progress in synthesis and application of magnetic carbon nanocomposites, Nanoscale 3 (2011) 2748-2767.
[20] R.K. Sharma, S. Dutta, S. Sharma, R. Zboril, R.S. Varma, M.B. Gawande, Fe_3O_4 (iron oxide)-supported nanocatalysts: synthesis, characterization and applications in coupling reactions, Green Chem. 18 (2016) 3184-3209.
[21] M.B. Gawande, Y. Monga, R. Zboril, R.K. Sharma, Silica-decorated magnetic nanocomposites for catalytic applications, Coord. Chem. Rev. 288 (2015) 118-143.
[22] M. Imran, D.H. Kim, W.A. Al-Masry, A. Mahmood, A. Hassan, S. Haider, S.M. Ramay, Manganese-, cobalt-, and zinc-based mixed-oxide spinels as novel catalysts for the chemical recycling of poly (ethylene terephthalate) via glycolysis, Polym. Degrad. Stab. 98 (2013) 904-915.
[23] G. Park, L. Bartolome, K.G. Lee, S.J. Lee, D.H. Kim, T.J. Park, One-step sonochemical synthesis of a graphene oxide–manganese oxide nanocomposite for catalytic glycolysis of poly(ethylene terephthalate), Nanoscale 4 (2012) 3879-3885.
[24] L. Bartolome, M. Imran, K.G. Lee, A. Sangalang, J.K. Ahn, D.H. Kim, Superparamagnetic γ-Fe_2O_3 nanoparticles as an easily recoverable catalyst for the chemical recycling of PET, Green Chem. 16 (2014) 279-286.
[25] W.L.F. Armarego, D.D. Perrin, Purification of laboratory chemicals, Butterworth-Heinemann, Oxford (UK), 1997.
[26] F. Galán-Cano, M.C. Alcudia-León, R. Lucena, S. Cárdenas, M. Valcárcel, Ionic liquid coated magnetic nanoparticles for the gas chromatography/mass spectrometric determination of polycyclic aromatic hydrocarbons in waters, J. Chromatogr. A 1300 (2013) 134-140.
[27] F.A. Casado-Carmona, M.C. Alcudia-León, R. Lucena, S. Cárdenas, M. Valcárcel, Magnetic nanoparticles coated with ionic liquid for the extraction of endocrine disrupting compounds from waters, Microchem. J. 128 (2016) 347-353.
[28] Y. Wang, X. Peng, J. Shi, X. Tang, J. Jiang, W. Liu, Highly selective fluorescent chemosensor for Zn^{2+} derived from inorganic-organic hybrid magnetic core/shell $Fe_3O_4@SiO_2$ nanoparticles, Nanoscale Res. Lett. 7 (2012) 86.

[29] H. Wu, G. Gao, X. Zhou, Y. Zhang, S. Guo, Control on the formation of Fe_3O_4 nanoparticles on chemically reduced graphene oxide surfaces, CrystEngComm 14 (2012) 499-504.
[30] P. Bender, C. Balceris, F. Ludwig, O. Posth, L.K. Bogart, W. Szczerba, A. Castro, L. Nilsson, R. Costo, H. Gavilán, D. González-Alonso, I. de Pedro, L. Fernández Barquín, C. Johansson, Distribution functions of magnetic nanoparticles determined by a numerical inversion method, New J. Phys. 19 (2017) 073012.
[31] F. Scé, I. Cano, C. Martin, G. Beobide, O. Castillo, I. de Pedro, Comparing conventional and microwave-assisted heating in PET degradation mediated by imidazolium-based halometallate complexes, New J. Chem. 43 (2019) 3476-3485.
[32] J. Sun, D. Liu, R.P. Young, A.G. Cruz, N.G. Isern, T. Schuerg, J.R. Cort, B.A. Simmons, S. Singh, Solubilization and upgrading of high polyethylene terephthalate loadings in a low-costing bifunctional ionic liquid, ChemSusChem 11 (2018) 781-792.
[33] N.D. Pingale, V.S. Palekar, S.R. Shukla, Glycolysis of postconsumer polyethylene terephthalate waste, J. Appl. Polym. Sci. 115 (2010) 249-254.
[34] Y. Yoshida, A. Otsuka, G. Saito, S. Natsume, E. Nishibori, M. Takata, M. Sakata, M. Takahashi, T. Yoko, Conducting and magnetic properties of 1-ethyl-3-methylimidazolium (EMI) salts containing paramagnetic irons: liquids $[EMI][M^{III}Cl_4]$ (M = Fe and Fe0.5Ga0.5) and solid $[EMI]_2[Fe^{II}Cl_4]$, Bull. Chem. Soc. Jpn. 78 (2005) 1921-1928.
[35] I. de Pedro, A. García-Saiz, J. González, I. Ruiz de Larramendi, T. Rojo, C.A.M. Afonso, S.P. Simeonov, J.C. Waerenborgh, J.A. Blanco, B. Ramajo, J. Rodriguez-Fernandez, Magnetic ionic plastic crystal: choline$[FeCl_4]$, Phys. Chem. Chem. Phys. 15 (2013) 12724-12733.
[36] I. de Pedro, O. Fabelo, A. García-Saiz, O. Vallcorba, J. Junquera, J.A. Blanco, J.C. Waerenborgh, D. Andreica, A. Wildes, M.T. Fernández-Díaz, J. Rodriguez-Fernandez, Dynamically slow solid-to-solid phase transition induced by thermal treatment of Dimim$FeCl_4$ magnetic ionic liquid, Phys. Chem. Chem. Phys. 18 (2016) 21881-21892.
[37] P. González-Izquierdo, O. Fabelo, G. Beobide, O. Vallcorba, F. Sce, J.F. Rodríguez, M.T. Fernández-Díaz, I. de Pedro, Magnetic structure, single-crystal to single-crystal transition, and thermal expansion study of the (Edimim)$[FeCl_4]$ halometalate compound, Inorg. Chem. 57 (2018) 1787-1795.
[38] J. Estager, J. D. Holbrey, M. Swadźba-Kwaśny, Halometallate ionic liquids – revisited, Chem. Soc. Rev. 43 (2014) 847-886.
[39] R.D. Tilve, M.V. Alexander, A.C. Khandekar, S.D. Samant, V.R. Kanetkar, Synthesis of 2,3-unsaturated glycopyranosides by Ferrier rearrangement in $FeCl_3$ based ionic liquid, J. Mol. Catal. A-Chem. 223 (2004) 237-240.
[40] M. Vasiloiu, P. Gaertner, K. Bica, Iron catalyzed Michael addition: chloroferrate ionic liquids as efficient catalysts under microwave conditions, Sci. China Chem. 55 (2012) 1614-1619.
[41] N.H. Ko, J.S. Lee, E.S. Huh, H. Lee, K.D. Jung, H.S. Kim, M. Cheong, Extractive desulfurization using Fe-containing ionic liquids, Energy Fuels 22 (2008) 1687-1690.
[42] J. Gao, Q.W. Song, L.N. He, C. Liu, Z.Z. Yang, X. Han, X.D. Li, Q.C. Song, Preparation of polystyrene-supported Lewis acidic Fe(III) ionic liquid and its application in catalytic conversion of carbon dioxide, Tetrahedron 68 (2012) 3835-3842.
[43] M.K. Leu, I. Vicente, J.A. Fernandes, I. de Pedro, J. Dupont, V. Sans, P. Licence, A. Gual, I. Cano, On the real catalytically active species for CO_2 fixation into cyclic carbonates under near ambient conditions: Dissociation equilibrium of $[BMIm][Fe(NO)_2Cl_2]$ dependant on reaction temperature, App. Catal., B 245 (2019) 240-250.
[44] M.H. Valkenberg, C. deCastro, W.F. Hölderich, Friedel-Crafts acylation of aromatics catalysed by supported ionic liquids, Appl. Catal., A 215 (2001) 185-190.
[45] J. Gao, J.-Q. Wang, Q.-W. Song, L.-N. He, Iron (III)-based ionic liquid-catalyzed regioselective benzylation of arenes and heteroarenes, Green Chem. 13 (2011) 1182-1186.